Experimentally Determined Structure of the Shock Reflection Process in Ionizing Xenon

Jerome A. Smith

Citation: The Physics of Fluids **11**, 2150 (1968); doi: 10.1063/1.1691797
View online: http://dx.doi.org/10.1063/1.1691797
View Table of Contents: http://aip.scitation.org/toc/pfl/11/10
Published by the American Institute of Physics

tion times were measured, may be justified in view of the almost straight line relationship in Fig. 2.

Furthermore, the local vibrational relaxation time $\tau_v(\tau)$ may be obtained from Eq. (6) in the following form:

$$1/k_{10}(0)\tau_v(\tau) = K_{10}(\tau)\ \{1 - \exp\ [-\theta(\tau)]\}. \quad (10)$$

Comparing Eq. (10) with Eq. (7), it is well known that for a constant heat-bath temperature where $f_1(T) = f_1(T_\infty)$, the slope $d \ln \mathcal{R}/d\tau$ represents directly the term $1/k_{10}(0)\tau_v$, or $d \ln \mathcal{R}/dt = 1/\tau_v$. However, for a variable heat-bath temperature, the slope $d \ln \mathcal{R}/d\tau$ differs slightly from the term $1/k_{10}(0)\tau_v(\tau)$ [or $d \ln \mathcal{R}/dt \neq 1/\tau_v(\tau)$] by a variable factor as shown in Eq. (7). Using the relation $K_{10}(\tau) = k_{10}(\tau)/k_{10}(0)$ and expressing all time-dependent variables in terms of the instantaneous heat bath temperature $T(\tau)$, one may write Eq. (10) as follows:

$$1/\tau_v(T) = k_{10}(T)\ \{1 - \exp\ [-\theta(T)]\}. \quad (11)$$

This indicates that $\tau_v(T)$ is a function of T only and is independent of the flow process where τ_v is measured or evaluated. If τ_v were evaluated from a certain flow process, τ_v should be plotted against the corresponding T of this flow process in the Landau–Teller diagram. Otherwise, errors will be introduced when, for example, τ_v is plotted against the average[7,8] temperature behind the shock or the measured equilibrium[6] temperature behind the shock while the constant enthalpy process was actually used by the above authors. However, in Hurle's[6] case, the equilibrium temperature for the constant enthalpy process is practically the same as the measured equilibrium temperature (for the constant total enthalpy process) as shown in the present example except for cases of much lower free-stream Mach numbers.[2]

ACKNOWLEDGMENT

This work was partially supported by the Engineering Research Institute, Iowa State University.

[7] V. Blackman, J. Fluid Mech. **1**, 61 (1956).
[8] R. C. Millikan and D. R. White, J. Chem. Phys. **39**, 98 (1963). The method of evaluation was discussed in Ref. 6.

THE PHYSICS OF FLUIDS VOLUME 11, NUMBER 10 OCTOBER 1968

Experimentally Determined Structure of the Shock Reflection Process in Ionizing Xenon

JEROME A. SMITH*
California Institute of Technology, Pasadena, California
(Received 20 December 1967; final manuscript received 6 June 1968)

The results of an experimental investigation of the reflection of strong shocks in xenon from the end wall of a shock tube are presented. The reflection of the incident shock structure, consisting of a frozen shock front, a region of relatively uniform frozen flow, and an ionization front, was observed with a fast-rise (0.3 μsec) pressure gauge mounted in the shock-tube end wall. The incident shock Mach number was varied from 11–20, and the initial pressure was varied from 0.1–1.5 mm Hg. The interaction between the reflecting shock and the ionizing gas in the incident shock structure produces a complicated series of shock and rarefaction waves; those waves that propagate back to the end wall were observed with the pressure gauge. A simple model which includes the gross features of the shock reflection process is used to calculate end wall pressures. The calculated pressures agree well with the experimental observations. In addition, ionization relaxation times for xenon behind the incident and reflected shocks are presented. The relaxation time data yield a better understanding of the ionization relaxation process in monatomic gases and provide an estimate for the electron–atom, inelastic cross section for xenon.

I. INTRODUCTION

In the present investigation a fast-rise pressure guage similar to the one developed by Baganoff[1,2] is used to measure the time history of the *pressure* on the end wall of a shock tube behind reflected shocks in xenon. The shocks considered are of sufficient strength to produce relatively high equilibrium degrees of ionization behind both the incident and reflected shocks, e.g., the equilibrium degree of ionization behind the incident shock varies from 0.07–0.45. Of particular interest is the manner in which the reflected shock interacts with the ionizing gas behind the incident shock. This interaction

* Present address: Gas Dynamics Laboratory, Princeton University, Princeton, New Jersey.
[1] D. Baganoff, Rev. Sci. Instr. **35**, 288 (1964).
[2] D. Baganoff, in *Proceedings of the Fifth International Shock Tube Symposium* (U. S. Naval Ordnance Laboratory, Silver Spring, Maryland, 1965), p. 195.

produces a complicated wave pattern, a series of shock and rarefaction waves; those waves which propagate to the end wall can be observed with the pressure gauge.

In this paper the term *shock* or *shock structure* denotes the transition region between one equilibrium state and another, i.e., including the region in which the internal degrees of freedom equilibrate. It will be useful to consider separately the part of the shock structure in which only the translational degrees of freedom are excited. This region is denoted by the term *frozen shock front.*

The structure of an ionizing shock in a monatomic gas is peculiar, in that the translational, or frozen, shock front is followed first by a region of practically constant density and then by a relatively rapid increase of density, practically a jump, in which the ionization level rapidly rises to the equilibrium value.[3] The "jump" is called the *ionization front.*[4] The density profile shown in Fig. 1 depicts this qualitatively. The interaction between the reflected shock and the ionization front produces a series of finite amplitude waves, some of which propagate back to the end wall and can be observed by the pressure gauge (Fig. 1). These waves are shown schematically in Fig. 1 and are labeled interaction waves. They will be described in more detail later, but we can see qualitatively that if the density increase across the ionization front were infinitely large, a shock would be reflected back towards the end wall. It then follows, e.g., from a pressure-velocity diagram, that a shock must be transmitted into the equilibrium gas in region 2*e*. While this qualitative argument appears to be similar to that used in a shock-contact surface interaction, the ionization front is neither a contact surface nor a shock front; it is simply part of the shock structure.[5]

This investigation does not represent the first attempt to describe the shock reflection process in ionizing monatomic gases. In their end-wall measurements of heat transfer rates in argon, Camac and Feinberg[4] observed a second sharp increase in heat transfer after the one due to the frozen incident shock reflection. This second heat transfer increase occurred at a time approximately equal to $\tau_{2\ \mathrm{ion}}$ (Fig. 1). They postulated that the interaction between the reflected shock and the ionization front behind the incident shock creates a disturbance,

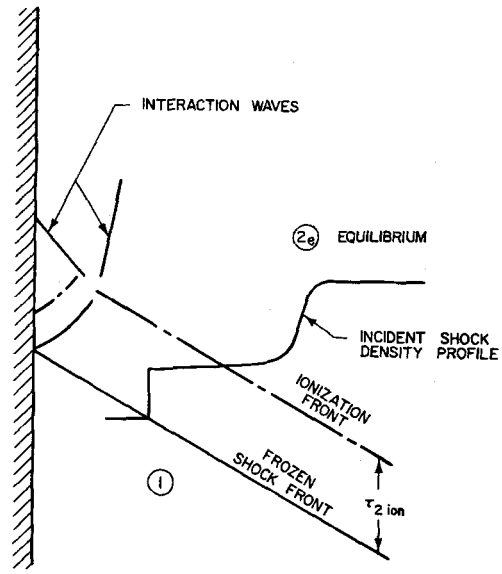

FIG. 1. Schematic shock reflection process for ionizing monatomic gas shock structure.

probably a shock, which propagates back to the end wall with approximately the same velocity as the incident shock. However, they were unable to give any more details about the *x-t* diagram for the shock reflection process, nor were they able to assess the strength of the wave which produced the second heat transfer rate increase from their measurements.

On the other hand, the end-wall pressure gauge can be used to measure the strength of the shock which results from the interaction. In addition, other waves which propagate to the end wall are observed with the pressure gauge, and the resulting pressure changes and arrival times (at the end wall) lead to a more complete understanding of the shock reflection process in highly ionized monatomic gases.

II. DESCRIPTION OF THE EXPERIMENTAL TECHNIQUE

These experiments were performed in the Graduate Aeronautical Laboratories, California Institute of Technology 6-in.-i.d. shock tube.[5,6] Room temperature hydrogen was used as a driver gas to produce incident shock Mach numbers ranging from 10.9–20.5 in xenon. The initial pressure was varied from 0.1–1.5 mm Hg; however, the bulk of the experimental data was obtained at an initial pressure of 0.5 mm Hg.

In order to avoid contamination of the test gas, the driven section was evacuated to a pressure of 0.03 μ Hg. (The initial *combined* leak and outgassing

[3] H. Wong and D. Bershader, J. Fluid Mech. **26**, 459 (1966).
[4] M. Camac and R. M. Feinberg, J. Fluid Mech. **21**, 673 (1965).
[5] J. A. Smith, Ph.D. thesis, California Institute of Technology (1967).
[6] J. A. Smith, D. Coles, A. Roshko, and A. J. Prasad, Graduate Aeronautical Laboratories, California Institute of Technology Report FM-67-1 (1967).

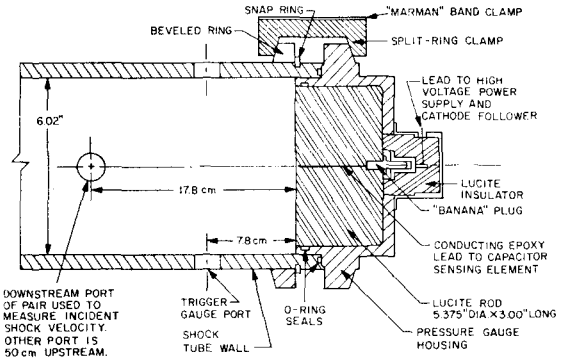

FIG. 2. Sectional view of end-wall pressure gauge in the Graduate Aeronautical Laboratories, California Institute of Technology 6-in. shock tube.

rate was less than 3.0 μ Hg/h.) The test gas was introduced within seconds after pumping ceased, and the run was completed a few minutes later.

Using a pressure gauge and a calibrated volume, the desired amount of xenon could be measured with an error less than 1%. This produces a 1% uncertainty in the end-wall pressure measurements.

The incident shock velocity for each run was determined by observing the response of two platinum thin film heat transfer gauges on an oscilloscope. The location of these heat transfer gauges with respect to the end-wall pressure gauge is shown in Fig. 2. A conservative estimate of the error in determining the incident shock Mach number M_s is $\pm 1\%$. This uncertainty affects the comparison between some of the measured and predicted pressure levels since a 1% variation in M_s produces a 2–3% variation in the predicted pressure levels.

A. The Pressure Gauge

The pressure gauge used to measure the pressure history on the wall of the shock tube was a larger diameter version of the type originally developed by Baganoff.[1] The principle of operation of the modified gauge is the same, but its performance is much better than that of Baganoff's original gauge. The modifications from which the present design resulted were made by Baganoff, while still at Caltech, with the author's assistance.[5]

Basically the gauge consists of a capacitor which is placed on the front surface of a cylindrical elastic rod of Lucite. The Lucite rod is visible in Fig. 2, but the plates of the capacitive sensing element, approximately 2.5-cm diameter, and the 0.12-mm thick Lexan dielectric material are not shown. (See Ref. 1 for the theory of operation of the gauge.)

The procedure for calibrating the pressure gauge, in order to obtain a pressure-voltage conversion factor, is the same as that outlined by Baganoff.[1] The sensitivity of the present gauge, determined from the calibration procedure, is 30.0 μV per mm Hg pressure change for each kV of charging voltage. A maximum of 6.5 kV was used with the present gauge, resulting in a maximum sensitivity of almost 0.2 mV/mm Hg. The rise time for this gauge is approximately 0.3 μsec. The end-wall pressure history is undistorted for 24 μsec. The distortion which begins after 24 μsec is due to stress waves propagating in from the radial boundary of the Lucite backing rod, causing the gauge to "ring."[1]

III. EXPERIMENTAL RESULTS

A. The Effect of the Ionized Gas on the Pressure Gauge

It was found that the response of the pressure gauge was affected by the presence of the ionized gas near the end wall. This "electrical effect" is reproducible and represents a 10% perturbation (approximately) on the actual pressure signal. The polarity of the voltage change associated with a pressure change is opposite to the polarity of the initial (charging) voltage on the capacitive sensing element, whereas the polarity of the "electrical effect" is *independent* of charging voltage polarity. Therefore, two runs with opposite polarity of charging voltage were made for each condition. By algebraically subtracting the response of one run from the other, a net pressure history was constructed.[7] This procedure was verified by comparing the results from a pair of runs at a lower incident shock Mach number, $M_s \simeq 10$, with the Rankine–Hugoniot jump for an ideal gas. For this condition the electrical effect was observed, but the gas was so weakly ionized that there could be no measureable effect on the end wall pressure history.[5] (No appreciable variation of the absolute magnitude of the "electrical effect" perturbation was observed when the magnitude of the shock Mach number or the magnitude of the charging voltage was varied.)

B. Typical Pressure Histories

The end-wall pressure histories resulting from a pair of runs in xenon with an incident shock Mach number $M_s = 15.1$ and an initial pressure $P_1 = 0.5$ mm Hg are shown in Fig. 3. The sweep speed in both oscillograms is the same, and time increases from left to right. The time markers on the traces

[7] Recently, a two-element gauge, which eliminates the need for making two runs in conditions where the "electrical effect" is important, has been developed. R. K. Hanson and D. Baganoff, (to be published).

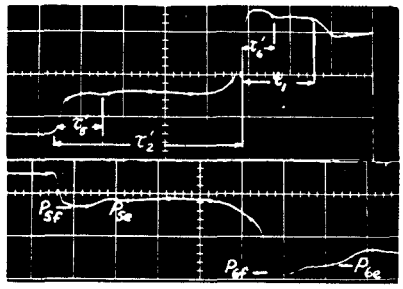

FIG. 3. Typical pair of runs showing end-wall pressure history in xenon; $M_s = 15.1$, $P_1 = 0.5$ mm Hg, sweep speed $\simeq$ 3.0 μsec/div, sensitivity 50 mV/div. Timing marks are 3.0 μsec apart.

are 3.00 μsec apart. On the upper oscillogram, which corresponds to a negative charging voltage, various time intervals of interest are noted. On the lower oscillogram, which corresponds to a positive charging voltage, various pressure levels of interest are noted. On the upper oscillogram a pressure increase is upward, and on the lower trace increasing pressure is downward. The "net" pressure history constructed from these two runs is shown next to the x-t diagram in Fig. 4. The assumptions made in order to construct the x-t diagram in Fig. 4 are described later (Sec. IV), but it is useful to consider Figs. 3 and 4 together when discussing the various pressure levels and time intervals observed.

The first pressure rise is due to the frozen incident shock front reflecting from the end wall. It is followed by a slight pressure increase resulting from the decay of the heat transfer perturbation which has been described elsewhere.[8,9] Before an asymptote for this initial pressure rise (P_{5f}) can be reached, the pressure begins to decrease slightly. This decrease is due to the ionization relaxation process behind the reflected shock. A minimum pressure (P_{5e}) is reached. (This is more apparent in the lower oscillogram in Fig. 3 since the "electrical effect" tends to mask this change in the upper one.) The time interval, denoted by τ_5' is related to the ionization relaxation time behind the reflected shock, and *is determined at the minimum pressure point.*

Following the relaxation to equilibrium behind the reflected shock, the pressure remains almost constant. Then, there is an abrupt pressure increase ($P_{5e} \rightarrow P_{6f}$). This pressure increase is the most interesting part of the end-wall pressure history. It arises from the interaction between the reflecting shock and the ionization front behind the frozen incident shock front (Fig. 4). This interaction

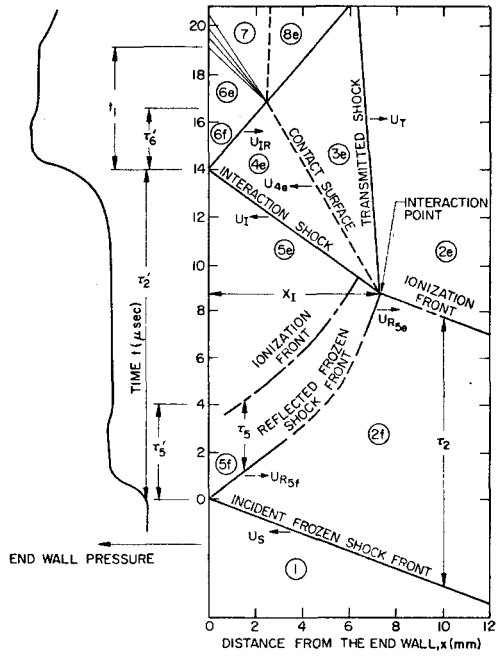

FIG. 4. x-t diagram for shock reflection process in xenon; $M_s = 15.1$ mm Hg. $P_1 = 0.5$ mm Hg.

produces a weak shock that propagates back to the end wall. (This shock is *weak* in the sense that the pressure ratio P_{6f}/P_{5e} is approximately three.) Thus, the time τ_2' is related to the ionization relaxation time τ_2 behind the frozen incident shock front. τ_2' *is determined at the midpoint of the second pressure rise.*

Following the maximum pressure point (P_{6f}), the pressure decreases slightly to a constant level (P_{6e}). This is terminated by a sharper, though small, pressure decrease.

The other times τ_6' and t_1 are best described by observing the oscillograms in Fig. 5, which are the results from a series of runs in which the initial conditions (pressure, temperature, and density) were kept constant while the Mach number was varied. All of these oscillograms have the same sweep speed and all correspond to a negative charging voltage on the pressure gauge. It is instructive to examine this series because the dependence on initial density in the relaxation phenomena has been removed. This means that the time scale changes on the complicated shock reflection process are due only to changes in temperature.

Various time intervals have been indicated on the oscillograms in Fig. 5. The first two τ_5' and τ_2', correspond to the "relaxation times" described above. As expected these two time intervals decrease with increasing temperature (Mach number).

[8] D. Baganoff, J. Fluid Mech. **23**, 209 (1965).
[9] F. A. Goldsworthy, J. Fluid Mech. **5**, 164 (1959).

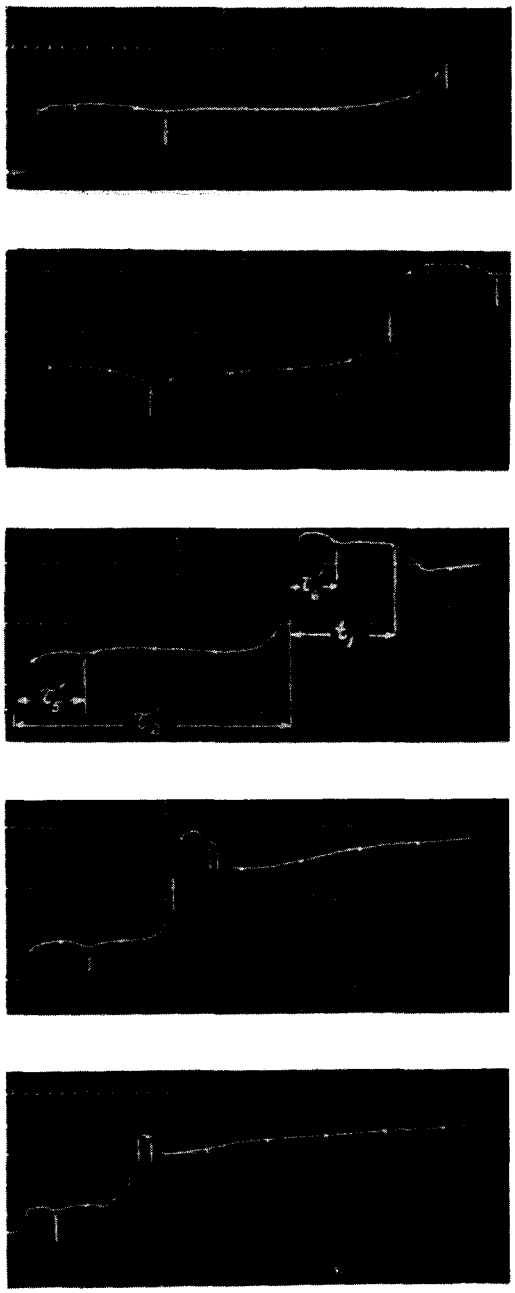

FIG. 5 A series of end-wall pressure histories in xenon; P_1 = 0.5 mm Hg. Timing marks are 3.0 μsec apart. From top to bottom, M_s = 13.5, 14.0, 15.1, 16.2, and 17.9.

The third time indicated, τ_6', denotes the slight pressure decrease ($P_{6f} \rightarrow P_{6e}$) behind the maximum pressure point. As the notation implies (subscripts f and e), this pressure change is associated with a relaxation process. Note the similarity between this pressure decrease and that due to the ionization behind the frozen reflected shock front ($P_{5f} \rightarrow P_{5e}$). Thus, τ_6' is considered to be a measure of the relaxation time behind this second reflecting shock; it can be observed to decrease as the Mach number increases. The fourth time interval, denoted by t_1, (visible on the lower three oscillograms only) indicates the arrival of a weak rarefaction pattern at the end wall. The values of t_1 and τ_2' taken from the oscillograms have been used to construct the x-t diagram for the shock reflection process in Fig. 4.

IV. ASSUMPTIONS USED TO CONSTRUCT THE x-t DIAGRAM FOR THE SHOCK REFLECTION PROCESS

The peculiar nature of the ionization relaxation process in a monatomic gas such as xenon, i.e., a relaxation process consisting of almost discontinuous changes in contrast to the gradual changes observed for vibrational relaxation,[8] permits some simplification in the description of the shock reflection process.

The model for the incident shock structure consists mainly of two simple elements, the frozen shock front and the ionization front, separated by a region of uniform frozen flow. This simplification is justified by (1) the incident shock density profiles for argon[3]; (2) the qualitatively similar ionization relaxation process for argon and xenon, observed during the initial, atom–atom, phase of the relaxation process[10,11]; (3) the similarity between the end-wall heat transfer histories in argon[4] and xenon[12] and (4) a numerical analysis of the relaxing gas within the incident shock structure in xenon. (The numerical analysis, made in connection with some of the relaxation times measured in this investigation, is described elsewhere.[5]) Therefore, the gas in region 2f (Fig. 4) is assumed to be completely frozen, and the gas in region 2e is assumed to be in equilibrium. Conditions in these two regions are conveniently tabulated elsewhere.[13,14]

Initially, the frozen reflected shock front leaves the wall with the velocity $U_{R_{sf}}$, corresponding to that for an ideal gas. [Conditions in region 5f may be calculated with the steady flow, shock jump equations[15] using the equation of state for an ideal gas, ($\gamma = \frac{5}{3}$).] However, the lagging internal degrees of freedom of the gas act like a series of heat sinks distributed in the vicinity of the reflected shock ionization front. This heat sink distribution creates

[10] K. E. Harwell and R. G. Jahn, Phys. Fluids **7**, 214, 1554 (1964).
[11] A. J. Kelly, J. Chem. Phys. **45**, 1723 (1966).
[12] H. S. Friedman and J. A. Fay, Phys. Fluids **8**, 1968 (1965).
[13] J. N. Mueller, NACA-Technical Note 4063 (1957).
[14] R. J. Arave, Boeing Report D 2-22291 (1963).
[15] H. W. Liepmann and A. Roshko, *Elements of Gas Dynamics* (John Wiley & Sons, Inc., New York, 1957), p. 388.

a rarefaction pattern which overtakes the frozen reflected shock front, causing it to decelerate, and it reduces the pressure on the end wall ($P_{5f} \rightarrow P_{5e}$).

Thus, even though the gas behind the reflected shock ionization front is in chemical equilibrium, it is in a nonuniform region because the gas has passed through a shock of varying strength. However, the degree of nonuniformity cannot be too severe since the end-wall pressure histories show that the pressure is almost constant (for $\tau_5' \leq t \leq \tau_2'$), and the equilibrium temperature is a very weak function of the reflected shock velocity, e.g., the value of T_{5e} increases by only 25% when the incident shock Mach number is increased from 10–20. Therefore, in our simplified model, it is assumed that the gas behind the reflected shock ionization front is in a uniform condition. The largest error in this assumption is that the reflected shock structure does not attain its equilibrium velocity $U_{R_{5e}}$ until just before ($t \lesssim \tau_2$) it interacts with the incident shock ionization front. Nevertheless, for the reasons just given, the gas properties in the region labeled 5*e* are given approximately by the equilibrium, steady flow, shock jump equations[15] corresponding to a reflected shock moving with velocity $U_{R_{5e}}$ into a uniform frozen gas (region 2*f*).[16]

In Fig. 4 the interaction occurring between the reflected shock structure S_{2f-5e} and the ionization front I_{2f-2e}[17] is shown as occurring at a point, the interaction point; however, the ionization front and the reflected shock structure both have a sigficant thickness so that the interaction *point* is actually a diffuse interaction *region*. The interaction shock S_{5e-4e} and the transmitted shock S_{2e-3e} are assumed to emerge from this interaction region and propagate into regions 5*e* and 2*e*, respectively.[18] For the purpose of determining the gross features of the shock reflection process, particularly for determining the pressures on the end wall, the details of this interaction are not important. (In Fig. 4 the ionization front behind the frozen reflected shock front is depicted as terminating on the line representing the trajectory of the shock S_{5e-4e}. This is just a schematic representation of what is actually taken to be part of the interaction region.)

The gas in regions 3*e* and 4*e* is assumed to be in an equilibrium, uniform condition since the high temperatures (~12 000°K) and electron number densities ($\sim 2 \times 10^{16}$ cm^{-3}) ahead of the shocks S_{5e-4e} and S_{2e-3e} imply that the relaxation times must be very short (~0.1 μsec).

A unique solution for conditions in regions 3*e* and 4*e* is defined by the fact that the pressure and flow velocity must be the same on either side of the contact surface C_{3e-4e}. A pressure-velocity diagram for the shock reflection process was used to compute conditions in regions 3*e* and 4*e*.[5] The loci of all shocks propagating into regions 5*e* and 2*e* were calculated by assuming various values of U_I and U_T (Fig. 4) and solving the conservation equations with the use of a Mollier diagram. The intersection of these locii on the pressure-velocity diagram determined the pressure and flow velocity in regions 3*e* and 4*e*.

In the discussion of Fig. 5, it was observed that the pressure decrease ($P_{6f} \rightarrow P_{6e}$) just behind the maximum pressure point in every way appeared analogous to the pressure decrease behind the frozen reflected shock front ($P_{5f} \rightarrow P_{5e}$). On the other hand, for these conditions the relaxation time behind the shock S_{4e-6f} should be extremely small, and one should only see the single pressure level P_{6e}. The most plausible explanation for this is that the cold wall inhibits the relaxation process inside the thermal layer, with the result that the gas first reaches equilibrium near the outer edge of the thermal layer. It then takes a finite time ($\sim\tau_6'$) for the pressure signal resulting from the relaxation process in the "free stream" to propagate back through the thermal layer and be observed on the end wall.

An estimate of the pressure P_{6f} is obtained by assuming that the gas composition is frozen across the shock S_{4e-6f}. The steady flow, shock jump equations are used, assuming that the gas is an inert mixture of atoms, ions, and electrons.[5]

The conditions in region 6*e* are calculated in much the same way as are conditions in regions 3*e* and 4*e*. In this case, however, the fact that the particle velocity u_{6e} is zero makes the calculation easier. The shock velocity U_{IR} used to construct the *x-t* diagram in Fig. 4 is the equilibrium shock velocity.

The arrival time of S_{5e-4e} at the end wall ($t = \tau_2'$) is determined experimentally. Similarly, the measured pressure history gives the arrival time of the leading edge of the rarefaction R_{6e-7} ($t = \tau_2' + t_1$).

[16] Reference 14 could have been used to make these and the other "real" gas calculations, but it was more convenient and accurate to use a Mollier diagram prepared at Aerospace Corporation since it had much smaller increments of temperature. This Mollier diagram was lent to the author through the courtesy of Dr. Alan F. Klein.

[17] In this and the discussion which follows, the symbols *I* and *S* denote an ionization front and a shock front, respectively. The subscripts refer to the regions ahead and behind the front.

[18] The finite thickness (in time) of the pressure rise $P_{5e} \rightarrow P_{6f}$ observed with the pressure gauge may indicate the structure of I_{2f-2e}, the structure of S_{5e-4e}, or a combination of the two. S_{5e-4e} is a *weak* shock or a series of compression waves because $P_{4e}/P_{5e} \leq 2$.

TABLE I. Summary of pressure gauge measurements for $P_1 \neq 0.5$ mm Hg.

M_s	P_1 mm Hg	$(P_{5f}/P_1)_{th}$	$(P_{5f}/P_1)_{exp}$	$(P_{5e}/P_1)_{th}$	$(P_{5e}/P_1)_{exp}$	$(P_{6f}/P_1)_{th}$	$(P_{6f}/P_1)_{exp}$	$(P_{6e}/P_1)_{th}$	$(P_{6e}/P_1)_{exp}$
12.6	1.500	1200	1100	925	1030	2100	2400	1940	2230
13.3	1.000	1320	1220	1010	1110	2675	2960	2450	2760
13.9	0.750	1440	1440	1095	1160	3250	3600	2920	3330
16.5	0.250	2030	1860	1520	1440	6720	6820	6100	6010
16.9	0.200	2120	2040	1590	1400	7300	7670	6720	6200[a]
18.3	0.100	2470	2310	1850	1850	9750	10400		[a]
20.4	0.100	3100	2770	2300	2020	14500	15100		[a]

[a] Rarefaction R_{6e-7} arrived at the end wall before pressure decreased to P_{6e}, i.e., no plateau present on oscillograms.

These two times τ_2' and t_1 *cannot be derived* even though the velocities U_I, U_{IR}, u_{4e}, and a_{6e} are known, since the trajectory of the reflected shock, S_{2f-5e}, is not known. (The leading edge of R_{6e-7} is assumed to propagate with the equilibrium speed of sound, a_{6e}.[14]) Therefore, in order to construct the x-t diagram in Fig. 4 and determine the interaction point, it was necessary to use the experimentally determined values of τ_2' and t_1. (In Fig. 3 one can see that τ_2' varied from run to run for the same initial conditions. This variation in τ_2' is discussed later. The value of τ_2' on the upper trace in Fig. 3 was used to construct Fig. 4. Variations in τ_2 alter the scale of the x-t diagram, but they do not affect the magnitude of the end-wall pressures observed.)

The difference between the times τ_5' and τ_5 shown in Fig. 4 is discussed below.

V. COMPARISON OF THE EXPERIMENTAL AND THEORETICAL RESULTS

A comparison of the theoretically predicted pressure levels and those observed experimentally is presented in Fig. 6. Since the pressure ratios P_{5e}/P_1, P_{6f}/P_1, and P_{6e}/P_1 are weak functions of the initial pressure, P_1, a constant initial pressure of 0.5 mm Hg was used for the theoretical and experimental values shown in this figure. The theoretical and experimental values for conditions at different initial pressures are summarized in Table I.

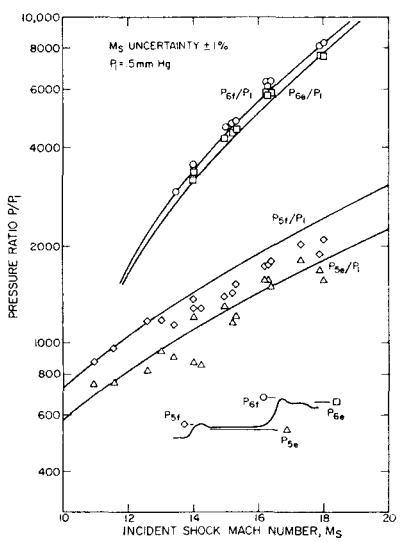

FIG. 6. Summary of end-wall pressure data.

The measured values of P_{5f} are as much as 20% below the corresponding predicted values. This is due to heat transfer to the end wall, which produces a negative pressure perturbation.[8,9] It can be shown[5] that for xenon the heat transfer perturbation persists for a time that is of the same order as the relaxation time τ_5 for $M_s \gtrsim 12.5$. In other words, the asymptotic ideal gas pressure level P_{5f} is not reached before the pressure begins to decrease (to P_{5e}) as a result of the relaxation process behind S_{2f-5f}. However, for $M_s \lesssim 12.5$ the observed values of P_{5f} do agree with the ideal gas predictions.

The observed values of P_{5e} agree with the theoretical predictions to within $\pm 10\%$ for all cases except the two data points at $M_s = 14.0$ (Fig. 6). A conservative estimate of the uncertainty in the experimentally determined magnitudes of P_{5f} and P_{5e} is $\pm 7\%$. This estimate does not include the $\pm 1\%$ uncertainty in the measured value of M_s, which is noted separately in Fig. 6, but it does include consideration of errors made in (1) measuring the initial pressure, (2) determining the calibration constant of the pressure gauge, and (3) measuring the amplitude of the pressure jump from the oscillograms.

The observed values of P_{6f} and P_{6e} are within 10% of the theoretical predictions, the majority of the experimental points lying slightly above the predicted values. The uncertainty in the measured values is estimated to be less than $\pm 5\%$. The single data point for P_{6f} in Fig. 6 at $M_s = 13.5$ is more uncertain because it could not be ascertained whether the asymptotic value of P_{6f} had been reached within the dwell time of the pressure gauge. (See the top oscillogram in Fig. 5.) Also, the values of P_{6e} for the

last three cases in Table I could not be determined experimentally because the rarefaction R_{6e-7} arrived at the end wall before the pressure level P_{6e} was established. An example where this almost occurred may be seen in Fig. 5 for the case $M_s = 16.2$.

In view of the adequate agreement between the predicted and the observed end-wall pressures, it may be concluded that the simple models for the ionizing shock structure and the interaction during reflection adequately describe the gross features of the phenomena observed.

VI. THE SHOCK REFLECTION PROCESS FOR TIMES LARGER THAN τ_2

Although it is not indicated in Figs. 1 and 4, this complicated interaction process must eventually decay. In other words, when viewed from infinity (time), the shock reflection process must look qualitatively like the reflection of a finite thickness translational shock, for example. By analyzing the subsequent interaction of S_{3e-8e} with S_{2e-3e} on the pressure-velocity diagram, it has been shown[5] that, for all practical purposes, the reflection process is complete after this interaction. The shock S_{3e-8e} overtakes S_{2e-3e} at a time $t \simeq 2\tau_2$ and produces a transmitted shock of a strength which is approximately equal to that one would calculate assuming a constant velocity shock propagates into region $2e$ with a uniform, equilibrium, zero-particle velocity region behind it. Any other interactions after this time must be extremely weak and cannot be described within the accuracy of the present model. In this respect, this reflecting ionizing shock structure is similar to that observed for reflecting translational and vibrational shock structures[8] in that the reflection is essentially complete within a few incident shock thicknesses. The relevant shock thickness in this case is τ_2.

VII. RELAXATION TIME DATA

To determine the time to reach equilibrium behind the incident shock in *laboratory coordinates* (τ_2), the measured values of τ_2' and t_1 have been used to calculate τ_2 using the relationship

$$\tau_2 = \tau_2' - X_I\left(\frac{1}{U_I} - \frac{1}{U_s}\right), \qquad (1)$$

where

$$X_I = \frac{U_I}{U_I - u_{4e}}\left[u_{4e} + \frac{U_{IR}(a_{6e} - u_{4e})}{U_{IR} + a_{6e}}\right]t_1. \qquad (2)$$

a_{6e} is the equilibrium velocity of sound in region $6e$. All the other quantities are indicated in Fig. 4. For the range of incident shock Mach numbers considered here, τ_2 is approximately $0.85\tau_2'$.

Ionization relaxation times behind incident shocks in xenon have previously been measured by other investigators. The maximum incident shock Mach number in any of those investigations was 11.0, so that comparison with most of our results is difficult. However, our values of $P_1\tau_2$ at $M_s = 11.0$[19] are more than a factor of 5 larger than those reported by Roth and Gloerson[20] and more than a factor of 2 larger than those reported by Turner.[21]

As a check on our method, a second technique was available for measuring the relaxation times for xenon behind the incident shock. This has been described by Klein,[22] who used a photomultiplier tube to monitor the onset of radiation behind the frozen incident shock front. It is known that this technique gives the relaxation time in monatomic gases with fairly good accuracy.[23] Klein's data were obtained in the same shock tube, and much of it even on the same runs as the pressure gauge data. A comparison between the present results for τ_2 and the values measured by Klein for an initial pressure $P_1 = 0.5$ mm Hg is shown in Fig. 7. Also shown in Fig. 7 are a few additional values of relaxation time measured by the author using the same technique as Klein. The close agreement between the relaxation times measured with a photomultiplier and those measured with the pressure gauge serves as further confirmation of Eqs. (1) and (2), and thus, confirms our model for the shock reflection process Fig. 4.

A. The Effect of Impurities on the Measured Relaxation Times

The scatter in the data in Fig. 7 and in other results obtained by Klein[22] (which are not shown in Fig. 7) indicate that impurities may effect the relaxation times measured. Using a photomultiplier to determine the onset of radiation behind the frozen incident shock front, Klein was not limited to the relatively small observation time (24 μsec) of the pressure gauge. As a result, he was able to obtain relaxation times over a wider range of initial

[19] Data obtained with a phototube, see the following discussion.
[20] W. Roth and P. Gloerson, J. Chem. Phys. 29, 820 (1958).
[21] E. B. Turner, Ph.D. thesis, University of Michigan (1956).
[22] A. F. Klein, Ph.D. thesis, California Institute of Technology (1967).
[23] H. E. Petschek and S. Byron, Ann. Phys. (N. Y.) 1, 270 (1957).

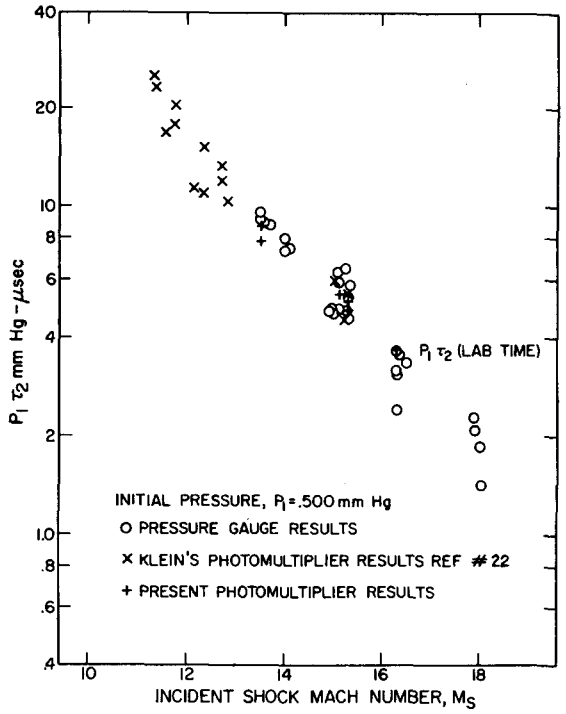

FIG. 7. Comparison of relaxation times measured with photomultiplier and with pressure gauge.

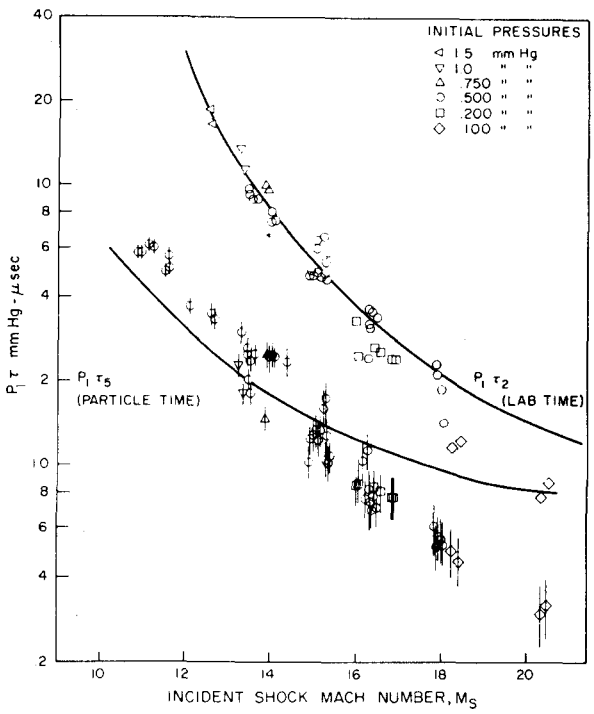

FIG. 8. Comparison between experimental results and predicted values of $P_1\tau_5$ using Eq. (4).

pressures, particularly for $M_s \lesssim 15$. His data show an "impurity effect," i.e., at the lower incident shock Mach numbers, values of $P_1\tau_2$ for $P_1 = 0.1$ mm Hg are approximately half the values of $P_1\tau_2$ obtained at the same Mach number with $P_1 = 0.5$ mm Hg. Unfortunately, Klein did not measure relaxation times for initial pressures greater than 0.5 mm Hg so that no estimate for the upper bound on $P_1\tau_2$ at any incident shock Mach number can be made from his data.

The relaxation times measured with the end-wall pressure gauge show a similar effect (see Figs. 8 and 9), although it is not nearly as pronounced because higher initial pressures and higher incident shock Mach numbers were used (in order that τ_2' be less than the 24 μsec observation time of the pressure gauge). However, the fact that the data points for $M_s \simeq 13.0$ for initial pressures of 1.0 and 1.5 mm Hg fall very close to a curve fitted through the $P_1 = 0.5$ mm Hg data points (Fig. 9) suggests that the relaxation times measured for initial pressures of 0.5 mm Hg or more are independent of impurity effects to within ±30% in the 6-in. shock tube.

The "impurity effect" is not nearly as evident in the measured values of $P_1\tau_5'$ [5] because of the larger scatter in these data. Two sources of this larger scatter are: (1) τ_5' is obtained by locating a small pressure perturbation on the oscillograms. This perturbation may be distorted by the so-called "electrical effect" on the pressure gauge. (2) There is some uncertainty in the values of τ_5' due to lack of time resolution on the oscillograms. This produces an uncertainty of approximately ±10%. Furthermore, in the next section it will be shown that the "relaxation time" τ_5' must be corrected for the effect of the end-wall thermal layer, and this introduces some additional uncertainty in these values, particularly for $M_s \geq 16$.

B. The Effect of the End-Wall Thermal Layer

Since the end wall stays at essentially room temperature, a thermal boundary layer develops at the wall behind the frozen reflected shock front. The cooler gas in the thermal layer does not ionize as rapidly as the gas that is not affected by the presence of the cold wall. The pressure gauge *does* observe a pressure change associated with the relaxation process ($P_{5f} \rightarrow P_{5e}$). But, since this occurs first near the "edge" of the thermal layer, and it takes a finite time for the sound wave, carrying the pressure change, to propagate through the thermal layer, there must be a time difference between the time that the gas first ionizes and when it is first observed on the end wall.

An x-t diagram of this phenomenon, shown in

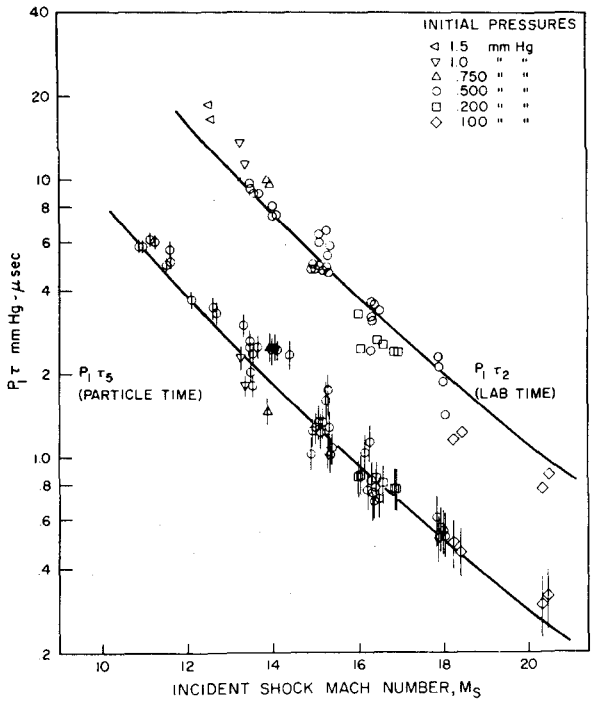

FIG. 9. Comparison between experimental results and predicted values of $P_1\tau_5$ using Eq. (11).

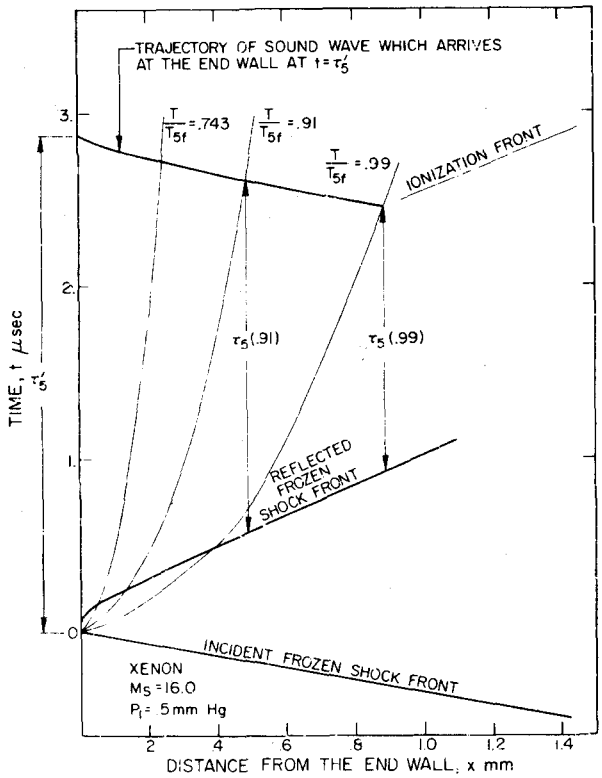

FIG. 10. x-t diagram showing the effect of the end-wall thermal layer on the measured relaxation time τ_5'.

Fig. 10, was constructed by integrating Goldsworthy's similarity solution.[9] The details of the assumptions used to make this calculation are described elsewhere.[5]

In Fig. 10 the line arriving at the end wall at $t = \tau_5'$ is the trajectory of a sound wave. The "relaxation time" seen by the pressure gauge is τ_5', but by following the trajectory of the sound wave to the edge of the thermal layer ($T/T_{5f} \simeq 0.99$), one can see that the actual relaxation time τ_5 may be considerably less than τ_5'. Therefore, all the experimental data should be reduced by an appropriate factor.

An uncertainty exists as to where, near the edge of the thermal layer, the gas ionizes first and produces the pressure change observed on the end wall. (Note that even though the gas at the 90% temperature point is at a lower temperature than T_{5f}, the gas there has been at a high temperature for a longer time than the gas at the 99% temperature point.) Added uncertainty is introduced by lack of knowledge of the coefficient of thermal conductivity and by the unknown effect of the very slightly ionized gas in region $2f$ on the relaxation process behind the reflected shock.

A reasonable assumption which includes all these uncertainties in determining the proper reduction factor is to assume that the gas first ionizes somewhere between the 90% and the 99% temperature points of the thermal layer (on the sound wave trajectory in Fig. 10). This estimate shows that $\tau_5 \simeq 0.9\tau_5'$ for $M_s = 11$, and $\tau_5 \simeq 0.6\tau_5'$ for $M_s = 18$. The corrected values, τ_5, are shown in Figs. 8 and 9. The ends of the vertical lines through the data points correspond to the 90% and the 99% temperature points and denote the uncertainty in the data due to the lack of knowledge of the proper reduction factor.

VIII. CORRELATION OF THE INCIDENT AND REFLECTED SHOCK RELAXATION TIME DATA

In the past a function of the form[4,12]

$$P_1\tau_{2_{lab}} = A \exp (T^*/T_{2f}) \qquad (3)$$

has been used to fit existing incident shock relaxation time data in order to estimate values of $P_1\tau_2$ at higher temperatures. (A and T^* are constants determined from the experimental data.) Correspondingly, the relaxation time behind the reflected shock is assumed to be given by the expression

$$P_1\tau_5 = A(\rho_{2f}/\rho_1)(\rho_{2f}/\rho_{5f}) \exp (T^*/T_{5f}), \qquad (4)$$

where the density ratio ρ_{2f}/ρ_1 converts τ_2 from laboratory time to particle time, and the factor

ρ_{2f}/ρ_{5f} accounts for the increased density behind the reflected shock.

Using the method of least squares, Eq. (3) has been fitted to the present data (A = 0.252 mm Hg-μsec, T^* = 65 200 °K). The results of this fit, as well as the corresponding prediction for $P_1\tau_5$, from Eq. (4), are shown in Fig. 8. The predicted values of $P_1\tau_5$ agree with the observed values for $M_s \simeq 15$, but at $M_s \simeq 18$ the predicted values are a factor of two larger than the experimental ones.

Aside from this lack of good correlation between τ_2 and τ_5, it is a disturbing fact that the temperature T^* does not correspond to any characteristic temperature or energy level for the ionization process in xenon. Similar empirical fits to measured relaxation times in argon[4,12] also do not give values of T^* that correspond to any characteristic energy level for the ionization process. In an attempt to resolve the question concerning T^* in Eqs. (3) and (4), a numerical calculation of the incident shock relaxation process in xenon was undertaken.

Calculating the Incident Shock Relaxation Process

The numerical solution was based upon theoretical considerations similar to those described for argon.[3,23,24] Details of the calculation procedure and the assumptions made are described elsewhere.[5]

The two major contributors to the production of electrons are collisions between atoms and collisions between electrons and atoms. A two-step ionization process has been observed[10,11] for the inelastic collisions between atoms and other atoms. By two-step process we mean that the atom is first excited to the first resonance state (8.5 eV), or metastable state (8.3 eV) and subsequently ionized, with the excitation process assumed to be rate determining. It is assumed that the two-step process is also dominant for the inelastic electron–atom collisions since the average energy of the electrons, $\simeq$ 1 eV, is much lower than the excitation energy, $\simeq$ 8 eV.

Assuming that the atom–atom and electron–atom inelastic cross sections vary linearly with energy,

$$\sigma_{A-A\ \mathrm{inel}} = B_{A-A}(E_A - E_m), \tag{5a}$$

$$\sigma_{e-A\ \mathrm{inel}} = B_{e-A}(E_e - E_m), \tag{5b}$$

the rates of electron production may be written as follows[23,25]:

$$\left(\frac{dn_e}{dt}\right)_{A-A} = 2\left(\frac{E_m^3}{m_A\pi}\right)^{\frac{1}{2}} n_A^2 B_{A-A} \frac{(\beta_A + 2)\exp(-\beta_A)}{\beta_A^{\frac{3}{2}}}, \tag{6a}$$

$$\left(\frac{dn_e}{dt}\right)_{e-A} = 4\left(\frac{E_m^3}{2\pi m_e}\right)^{\frac{1}{2}} n_e n_A B_{e-A} \frac{(\beta_e + 2)\exp(-\beta_e)}{\beta_e^{\frac{3}{2}}}. \tag{6b}$$

n, m, and E are the symbols for number density mass, and translational energy, respectively, with the subscript denoting the particular specie. β_i is the ratio E_m/kT_i. (E_m = 8.3 eV corresponds to the potential of the first metastable state which Kelly[11] measured for the atom–atom excitation process; however, the first resonance state potential 8.5 eV was within his experimental uncertainty.) The electron temperature T_e is found as a function of the atom temperature T_A and the degree of ionization by equating the electron energy lost through inelastic collisions to the electron energy gained by elastic collisions with ions and atoms.[23] $B_{A-A} = 1.8 \times 10^{-20}$ cm^2/eV is taken from Kelly's measurements.[11] B_{e-A} was first estimated by comparing Ramsauer's measured total (elastic plus inelastic) electron–atom cross section to the elastic electron–atom cross section[26] for electron energies greater than 8.3 eV. This comparison yielded a value $B_{e-A} \simeq 5 \times 10^{-16}$ cm^2/eV; however, it can be shown that the relaxation time is not very sensitive to the magnitude of this cross section.[5]

The important features brought out by the numerical solution are (1) the electron–atom process becomes dominant after 15–20% of the total relaxation time has elapsed and (2) the electron temperature remains essentially constant and almost equal to the equilibrium temperature. (These two results are qualitatively the same as those obtained for argon.[3]) Hence, if any characteristic time is to be obtained from the rate equations, Eq. (6b) rather than Eq. (6a) should be used, and so the temperature to use should be that of the electrons and not that of the atoms and ions.

If we assume that the electron temperature T_e and the atom number density n_A are constant in the relaxation region, we can obtain a characteristic time from the rate equation (6b) because

$$n_e \sim \exp(t/\tau), \tag{7}$$

where

$$\tau \sim \frac{(\beta_e)^{\frac{3}{2}}\exp(\beta_e)}{n_A(\beta_e + 2)}. \tag{8}$$

[24] E. J. Morgan and R. D. Morrison, Phys. Fluids 8, 1608 (1965).

[25] S. Chapman and T. G. Cowling, *The Mathematical Theory of Non-Uniform Gases* (Cambridge University Press, New York, 1960), Chap. 5.

[26] H. S. W. Massey and E. H. S. Burhop, *Electronic and Ionic Impact Phenomena* (Oxford University Press, London, 1956), pp. 9, 91, 92, 95.

Since

$$n_A \simeq n_{A_{e,f}} = (\rho_{2f}/\rho_1)n_1 \simeq 4p_1/kT_1 = \text{const } P_1, \quad (9)$$

$$P_1\tau_2 = C\frac{(\beta_e)^{\frac{3}{2}}\exp(\beta_e)}{(\beta_e+2)}, \quad (10)$$

where C is a constant determined from the experimental data and $\beta_e = E_m/kT_e$. Usually, fitting the data with a function of this form is undesirable since the determination of β_e, i.e., of the electron temperature T_e requires knowledge of the inelastic, electron–atom cross section. However, the equilibrium temperature T_{2e} is approximately equal to the electron temperature behind the incident shock. Therefore, the equilibrium temperatures T_{2e} and T_{5e} can be used instead of the electron temperature in the relaxation time equations.

The use of equilibrium temperatures introduces an undesirable dependence on initial pressure. (T_{2e} and T_{5e} are weak functions of initial pressure.) Since most of these data were obtained for $P_1 = 0.5$ mm Hg, no conclusion about this initial pressure dependence has been ascertained.

The constant C in Eq. (10) was determined from the measured values of τ_2, $C = 6.15 \times 10^{-5}$ mm Hg-μsec. This value for C implies $B_{e-A} \simeq 10^{-16}$ cm^2/eV. With this single empirical constant, the equation

$$P_1\tau_5 = 1.1\left(\frac{\rho_{2f}}{\rho_{5f}}\right)\left(\frac{\rho_{2f}}{\rho_1}\right)C\frac{(E_m/kT_{5e})^{\frac{3}{2}}\exp(E_m/kT_{5e})}{[(E_m/kT_{5e})+2]} \quad (11)$$

can then be used to predict the values of $P_1\tau_5$. The factor (1.1) is added to Eq. (11) for the laboratory-to-particle time conversion. This factor was determined from the numerical calculation; it results from the fact that the density is not exactly the frozen density ρ_{2f} in the relaxation region.[5]

A comparison between the experimental results for $P_1\tau_5$ and those predicted by Eq. (11) is shown in Fig. 9. The agreement over the entire range of incident shock Mach numbers is much better than that obtained with Eqs. (3) and (4), cf. Fig. 8, and this in spite of the fact that we use only *one* unknown constant, determined from the experimental data. Thus, this method provides not only a more accurate but also a sounder basis for correlating relaxation times over a wide range of temperatures, whether it be behind the incident or the reflected shock.

IX. CONCLUSIONS

Owing to the observed similarities in the relaxation processes of noble gases such as argon, krypton, and xenon,[4,10–12] it is very likely that the shock reflection process in argon and krypton is qualitatively the same as that described here for xenon. For these ionizing monatomic gases ($M_s \gtrsim 10$), caution must be exercised when performing experiments on the shock tube end wall, since no region of uniform, equilibrium gas exists next to the end walls for any appreciable time until $t \gtrsim 2\tau_2$. After $t \gtrsim 2\tau_2$ the effects of radiation cooling and/or reflected shock-side wall boundary-layer interaction may have to be taken into account.

Furthermore, the procedure outlined above for correlating ionization relaxation times for xenon, using a function of the electron (equilibrium) temperature and not the atom or frozen gas temperature, should work as well for argon and krypton.

ACKNOWLEDGMENTS

The author would like to express his sincere appreciation to Professor Anatol Roshko for his many helpful discussions in the course of this investigation and in writing this paper. Discussions with Professor H. W. Liepmann aided in the completion of this work, and his assistance is gratefully acknowledged. Special thanks go to Dr. Donald Baganoff for his patient instruction in the construction and use of the pressure gauge.

The work in the Graduate Aeronautical Laboratories, California Institute of Technology 6-in. shock tube was supported by the National Aeronautics and Space Administration under Grant NsG 40-60.